

The Globular Cluster Systems in the Coma Ellipticals. III: The Unique Case of IC 4051

Sean C. Woodworth and William E. Harris

Department of Physics & Astronomy, McMaster University, Hamilton, Ontario L8S 4M1

Electronic mail: woodwrth, harris@physics.mcmaster.ca

ABSTRACT

IC 4051 is a giant E galaxy on the outskirts of the Coma cluster core. Using archival *HST* WFPC2 data, we derive the metallicity distribution, luminosity function, and spatial structure of its globular cluster system (GCS). The metallicity distribution derived from the $(V - I)$ colors has a mean $\langle \text{Fe}/\text{H} \rangle \simeq -0.3$, a near-complete lack of metal-poor clusters, and only a small metallicity gradient with radius. We tentatively suggest that the GCS has two roughly equal metallicity subcomponents, one centered at $[\text{Fe}/\text{H}] \sim 0.0$ and the second at $[\text{Fe}/\text{H}] \sim -1.0$, although their identification is blurred by the photometric uncertainties. The luminosity distribution (GCLF) has the standard Gaussian-like form observed in all other giant E galaxies, with a peak (turnover) at $V^0 = 27.8$, consistent with a Coma distance of 100 Mpc. The radial profiles of both the GCS and the halo light show an unusually steep falloff which may indicate that the halo of this galaxy has been tidally truncated. Lastly, the specific frequency of the GCS is remarkably large: we find $S_N = 11 \pm 2$, at a level which rivals M87 and most others in the central cD-type category, even though IC 4051 is not a cD or brightest cluster elliptical. This galaxy exhibits a combination of GCS characteristics found nowhere else. A formation model consistent with most of the observations would be that this galaxy was subjected to removal of a large fraction of its protogalactic gas shortly after its main phase of globular cluster formation, probably by its first passage through the Coma core. Since then, no significant additions due to accretions or mergers have taken place, in strong contrast to the central Coma galaxy NGC 4874.

Subject headings: Galaxies: Star Clusters; Structure; Evolution; Elliptical; Individual

1. INTRODUCTION

The Coma Cluster ($d \sim 100$ Mpc), as a rich Abell cluster, is the host environment for a huge range of E/S0 galaxies. Its two central supergiants, NGC 4874 and 4889, are among the very most luminous galaxies known, and the cluster has many other large ellipticals scattered throughout its ~ 1 -Mpc core region and well beyond. The globular cluster systems (GCSs) around these galaxies are well within reach of the HST cameras, and thus give us an extraordinarily rich range of target galaxies for comparative GCS studies. Coma also has important implications for the determination of the Hubble constant H_0 , since its large recession velocity (~ 7100 km s $^{-1}$) greatly exceeds any anticipated local peculiar motions, and it is situated at high galactic latitude ($b = +87.7$) nearly unaffected by foreground absorption,

IC 4051 is a giant E2 galaxy located $\simeq 14'$ east in projection from the center of Coma and has no luminous neighbors. With an integrated magnitude $V_T^0 = 13.20$, it is the fifth brightest elliptical galaxy within the 1° central region of Coma. Thus, IC 4051 presents a good opportunity to study the GCS of a more-or-less “normal” large elliptical. Baum et al. (1997) obtained the first deep WFPC2 exposures of IC 4051 with exactly this purpose in mind, but they limited their published analysis to only the photometry from the PC1 frame on which the galaxy was centered. However, considerably more information on the radial structure of the GCS, its specific frequency, and radial metallicity gradient are potentially available from the outer sections of the WFPC2 field. In this paper, we re-analyze the archival HST/WFPC2 frames from the Baum et al. (1997) program and discuss the global properties of the IC 4051 GCS using the entire body of data available in the raw exposures.

2. DATA ANALYSIS

The raw database comprises *HST*/WFPC2 observations taken on 1995 July 20/21 (Baum et al. 1997). Eight images totalling 20500 s (essentially, a sequence of full-orbit exposures) were taken through the *F606W* (wide *V*) filter, and two images totalling 5200 s were taken through the *F814W* (*I*) filter. The techniques in our data analysis are similar to those in Papers I and II of this series (Kavelaars et al. 2000; Harris et al. 2000), in which we analyzed the GCS around NGC 4874, the central cD giant. The first step was to register and combine the images to produce a master *V* and master *I* frame free of cosmic rays. An excellent color composite image constructed from the combined frames is published by Baum et al. For the PC1 frame, we produced a “flattened” image in which the overall elliptical contours of the central galaxy were modelled and then subtracted. In the WF2,3,4 fields, we generated an empirical model of the galaxy light by median filtering each

frame and subtracting the smoothed image from the original picture (after a preliminary star-finding and removal).

Our photometry was then carried out on the flattened master frames with the DAOPHOT II and ALLSTAR codes (Stetson 1992). The instrumental magnitudes returned by ALLSTAR were transformed to the standard V, I system via the equations derived by Holtzman et al. (1995),

$$V = m(F606W) - \overline{\Delta m} + 22.093 + 0.254(V - I) + 0.012(V - I)^2 + 2.5 \log(GR_i), \quad (1)$$

$$I = m(F814W) - \overline{\Delta m} + 20.839 - 0.062(V - I) + 0.025(V - I)^2 + 2.5 \log(GR_i), \quad (2)$$

where $m(F606W, F814W)$ are the instrumental magnitudes returned by ALLSTAR, and the $\overline{\Delta m}$ are constants which shifts these ALLSTAR psf magnitudes to the equivalent magnitude of the light within a $0''.5$ aperture. The mean value of Δm was determined empirically for each of the four WFPC2 fields from roughly ten moderately bright, isolated stars in each CCD, and applied to all our detected starlike images. The typical internal uncertainties in the mean Δm values were ± 0.02 mag.

It should be noted that at the distance of Coma, all globular clusters are easily starlike in appearance and thus these transformation equations normalized to the $0''.5$ aperture can strictly be applied to them. The calibration equation for V quoted above is the synthetic model transformation from Table 10 of Holtzman et al. (1995), while the equation for I is the observationally based one from their Table 7. If, instead, we had chosen their Table 10 model transformation for I , our resulting $(V - I)$ color indices would have ended up bluer by roughly 0.02 mag at the average color $(V - I) \simeq 1.2$ of the IC 4051 globular clusters (see below; this shift would have the effect of reducing the deduced cluster metallicities by $\Delta[\text{Fe}/\text{H}] = 0.1$).¹ When we add the internal uncertainties in the aperture corrections Δm , we estimate that the zeropoints of either the magnitude or color scales are uncertain to at least ± 0.03 mag.

Finally, as an internal check on the relative zeropoints of the V and I scales between the PC1 chip and the three WF chips, we inspected the mean $(V - I)$ color indices of the measured globular clusters in the annulus around the center of IC 4051 ($R \sim 10'' - 20''$) that overlapped the PC/WF boundary. We enforced the WF2,3,4 data in this annulus to

¹Baum et al. (1997) adopted the synthetic transformation for I from Table 10 of Holtzman et al., but used the specific curve for the color range $(V - I) < 1.0$. However, the majority of the globular clusters are somewhat redder than this, so that the transformation for $(V - I) > 1.0$ would have been preferable. The net result is to increase the small $(V - I)$ difference between their scale and ours by a further $\sim 0.02 - 0.03$ mag, although our *instrumental* color scale ($F606W - F814W$) agrees quite closely with theirs.

have the same mean color as those in the PC1 region by adjusting the I magnitudes (which are from much shorter exposures than V , thus internally more uncertain). The final result places our $(V - I)$ scale in agreement with the Baum et al. (1997) scale to within 0.03 mag, a level entirely consistent with the combined photometric uncertainties.

As was already evident from the Baum et al. (1997) study, IC 4051 has a populous GCS, which appears as a very obvious swarm of faint objects across the whole WFPC2 field. The main source of sample contamination is from very faint, compact background galaxies, with a (nearly negligible) contribution from Galactic foreground stars. A high proportion of the background galaxies can be eliminated through conventional radial-moment image analysis. For this purpose we used the r_1 radial moment as implemented in Harris et al. (1991),

$$r_1 = \left(\frac{\sum rI}{\sum I} \right), \quad (3)$$

which is an intensity-weighted mean radius for the object calculated over all pixels brighter than the detection threshold (see Harris et al. 1991). A straightforward plot of r_1 against magnitude then shows a well defined stellar sequence, with nonstellar objects scattering to larger r_1 . These classification graphs for the four CCDs in V are shown in Figure 1. The dashed lines indicate the adopted cutoffs applied to the measurements. Similar object classifications were applied to the I data (which, however, have shallower limits), with the final culled data lists containing 4058 objects in V and 1672 objects in $(V - I)$.

The faint-end completeness of our photometry was investigated through an extensive series of artificial-star tests on the master images. The procedure performed here was to add 500 artificial stars to each frame over a range of input magnitudes, measure these frames through the normal DAOPHOT sequence, and find out how many were recovered. Fifteen of these trials were carried out, with average resulting completeness fractions as displayed in Figure 2. Convenient fits to the raw points are provided by the Pritchett interpolation function,

$$f = \frac{1}{2} \left[1 - \frac{\alpha(R - R_{lim})}{\sqrt{1 + \alpha^2(R - R_{lim})^2}} \right]. \quad (4)$$

Table 1 summarizes the best-fit parameters to Equation 4 for each CCD and bandpass. In the Table, (V_{lim}, I_{lim}) are the magnitudes at which f drops to 0.5, and the parameter α controls the steepness of the falloff. The curves for all three of the outer chips (WF2,3,4) are nearly identical; for the inner PC1 chip, the limiting magnitudes are brighter, driven by the spread of the PSF over many more pixels and (for $R \lesssim 10''$) the brighter background light.

Lastly, Figure 3 shows how the photometric measurement uncertainties (also derived

from the ADDSTAR completeness tests) increase with magnitude. At the formal limiting ($f = 0.5$) magnitude, the rms uncertainty in the photometry reaches 0.15 mag. Wherever possible, we avoid dealing with any features of the data below that limit.

3. COLOR AND METALLICITY DISTRIBUTIONS

The distribution in colour of the globular clusters can be used to gain insight into the existence of multiple sub-populations in the GCS. Bimodal color distributions are found about half the time in gE galaxies (e.g., Kundu & Whitmore 1999; Neilsen & Tsvetanov 1999) and are often interpreted as relics of at least two major phases of star formation in the early history of the galaxy, whether by merger, accretion, or *in situ* processes. With the conventional “null hypothesis” for giant ellipticals that the clusters are all old ($\gtrsim 10$ Gy), the color index is primarily a tracer of cluster metallicity. The colour-magnitude distribution for the 1672 objects measured in both V and I is shown in Figure 4. At projected galactocentric radii larger than about $80''$, we found (see below) that the residual numbers of clusters dropped nearly to zero, so we adopt this outer region as defining a suitable “background” population.

To eliminate a few more contaminating objects, we reject objects bluer than $(V - I) = 0.74$ or redder than $(V - I) = 1.46$ (vertical dashed lines in Fig. 4). These colour limits generously include the range in colours of the known globular clusters in large galaxies (e.g., Harris 1996; Whitmore et al. 1995; Neilsen & Tsvetanov 1999). We also further limited the color sample to objects brighter than $V = 26.0$ to ensure high completeness at all colors.

A “clean” color distribution for the GCS was then obtained by subtraction of the background ($R > 80''$) color distribution, normalized to the same total area as the inner population. This procedure left a final total of 479 objects within the magnitude and color limits given above, with a net distribution over $(V - I)$ as shown in the histogram of Figure 5. The mean color of the sample is $\langle V - I \rangle = 1.12 \pm 0.01$ (internal uncertainty of the mean), with a dispersion of $\sigma_{V-I} = 0.13$. Subtracting an adopted foreground reddening $E(V - I) = 0.014$ and using the calibration of $(V - I)_0$ in terms of metallicity given in Paper II,

$$(V - I)_0 = 0.17 [\text{Fe}/\text{H}] + 1.15,$$

we then estimate that the IC 4051 GCS as a whole has $\langle \text{Fe}/\text{H} \rangle \simeq -0.3$. The peak position of this color distribution is quite similar to the metal-*rich* components in other giant ellipticals such as NGC 4472 (Geisler et al. 1996), M87 (Whitmore et al. 1995; Kundu et al. 1999), and other Virgo members (Neilsen & Tsvetanov 1999). However, the metal-*poor*

component which is usually found in these same galaxies at a mean color $(V - I) \sim 0.95$ or $[\text{Fe}/\text{H}] \sim -1.5$ (and which we found in the Coma cD NGC 4874; see Paper II) is entirely missing in IC 4051, or at very most is a fringe component buried in the wings of the main distribution.

We cannot place firm limits on the intrinsic dispersion $\sigma[\text{Fe}/\text{H}]$, since the mean observational measurement scatter over the sample is $\sigma_{V-I} \simeq 0.11$, comparable with the observed sample dispersion of ± 0.13 . Nevertheless, subtracting off the observational scatter in quadrature, we estimate roughly $\sigma_0[\text{Fe}/\text{H}] \simeq 0.4$, which is in close agreement (for example) with the value $\sigma[\text{Fe}/\text{H}] = 0.38$ found by Geisler et al. (1996) to fit each of the metal-rich and metal-poor components in NGC 4472. In the Milky Way, the well known bimodal MDF has been found to be fit by Gaussian functions with dispersions near 0.3 dex (Zinn 1985; Armandroff & Zinn 1988; Harris 2000). For IC 4051, a single Gaussian with the same mean and standard deviation as the sample (Fig. 5) matches the MDF with a $\chi^2 \simeq 14.6$ over 14 degrees of freedom, which provides no strong evidence for bimodality (but see below).

Trends of mean color with either galactocentric distance or magnitude were also searched for. Table 2 shows the mean color and dispersion in 0.5-magnitude bins from $V = 22.5$ to 26.0. These binned means reveal no significant change in color with luminosity. However, slightly more interesting features emerge in the graph of color versus radius (Figure 6). Binned mean colors, listed in Table 3, indicate no systematic change in color for $R \gtrsim 10''$, but within $10''$ the clusters are indeed slightly redder than the overall mean. The distribution in its entirety is barely suggestive of two sub-populations: one centered on $(V - I) \sim 1.2$ which is found at all radii; and a second, slightly bluer one centered near $(V - I) \sim 1.0$. The lack of bluer clusters within $R \lesssim 10''$ is then largely responsible for the inner color gradient of the whole sample mentioned above. Much stronger versions of this same effect have shown up in some other giant E or cD galaxies with far more obvious bimodal MDFs (e.g., Secker et al. 1995; Geisler et al. 1996; Lee et al. 1998; Ostrov & Forte 1998). In these, the different central concentrations of the metal-rich and metal-poor subsystems produce a steady outward change in the relative proportions of blue-to-red clusters with radius and thus a mean metallicity gradient.

Using Fig. 6 as a guide, we divided the sample of objects at $(V - I) = 1.07$ and tested the radial distributions of the bluer and redder halves. A standard Kolmogorov-Smirnov two-sample test indicated that their spatial distributions are significantly different (the redder half is more centrally concentrated) at the 99% level, suggesting to us that the inner gradient is indeed a real effect.

We therefore *very tentatively suggest* that the IC 4051 system may contain a bimodal

MDF in which the two modes are rather closely spaced in mean metallicity, thus heavily blurred out by the raw photometric measurement uncertainty. Numerical experiments with various two-component fittings of the entire MDF lead to models of the form shown in Figure 7. Here, a sample twin-Gaussian fit is shown in which the bluer (metal-poor) component is centered at $(V - I) = 1.00$ or $[\text{Fe}/\text{H}] \simeq -0.96$, the redder (metal-rich) one at $(V - I) = 1.17$ or $[\text{Fe}/\text{H}] \simeq +0.04$, both have dispersions $\sigma(V - I) = 0.10$, and the redder one contains about 55% of the total sample. The combined components now represent the total shape of the MDF better, with its modest skewness toward the red side (the total χ^2 is 12.6). The relative proportions of blue and red components, however, are quite uncertain (the formal uncertainties are ± 0.1 , but variations of factors of two in the proportions give scarcely different overall fits).

Clearly, this particular two-component model is only illustrative of the range of possibilities: the moderately small difference in color between the two components, and the very significant broadening of the MDF by photometric measurement uncertainty, do not justify more extensive analysis. However, it would clearly be of value to measure the MDF of this populous globular cluster system with a photometric index much more sensitive to metallicity than $(V - I)$, in which the subpopulations would be far more clearly revealed. A more sensitive color index would also permit establishment of the true mean $[\text{Fe}/\text{H}]$ with much less zeropoint uncertainty.

Lastly, it is worth comparing the mean colors of the GCS components to that of the halo *light* of the central galaxy. Mehlert et al. (1998) find $(V - I) \simeq 1.30$ at a projected radius $R = 10''$, increasing inward to $(V - I) = 1.35$ at the very center. This color range is distinctly redder than the typical levels $(V - I) \simeq 1.20 \pm 0.03$ for giant E galaxies (Buta & Williams 1995; Prugniel & Héraudeau 1998). The measured absorption line indices (Mg, Fe, $\text{H}\beta$) lead Mehlert et al. (1998) to conclude, in line with the integrated color, that the core of IC 4051 is extremely old and very metal-rich, perhaps as high as $[\text{Fe}/\text{H}] = +0.25$. However, the deduced metallicity from the line indices becomes lower at larger radii, dropping to an equivalent $[\text{Fe}/\text{H}] \sim -0.5$ for $R \gtrsim 20''$ (the effective radius r_e of the light profile), similar to the inner GCS. Mehlert et al. find that IC 4051 harbors an old, co-rotating core with an unusually large “break radius” (it is detectable out to $5''$ or 3.4 kpc) but which contributes $\lesssim 1\%$ of the total light of the galaxy. If this inner stellar disk is a signature of a dissipational merging event, it is likely to have occurred at early times.

4. THE LUMINOSITY DISTRIBUTION

As Baum et al. (1997) showed, the V photometry reaches faint enough to reveal the “turnover point” (peak frequency) in the globular cluster luminosity function (GCLF). By adding in the photometry from the WF chips, we have been able to double the total sample of clusters and thus improve the definition of the GCLF.

The distribution of all the detected objects classified as “starlike” and used to define the GCLF is shown in Figure 8. These are, quite evidently, strongly concentrated to the center of IC 4051 (much more so than in the GCS of the Coma supergiant NGC 4874; see Papers I and II). More or less arbitrarily, we take the region $R > 80''$ marked by the outer dashed line in Fig. 8, as defining the luminosity function of the background population, to be subtracted statistically from the inner ($10'' < R < 80''$) zone after correction for photometric incompleteness.

The results of this exercise for each of the four CCD chips separately are shown in Figure 9. Aside from the noticeably brighter completeness limit for the PC1 zone, no significant differences in the GCLF shape or turnover from place to place are evident. (The GCLF peak for the PC1 region shows an apparent peak fainter than $V \sim 28$, but this is fainter than the 50% completeness limit and so cannot be given much weight.) We therefore add all four sectors to form the composite GCLF shown in Figure 10. The numerical results in 0.3-mag bins are listed in Table 4: here, successive columns give (1) the V magnitude range of the bin (2) the number of detected starlike objects in the inner ($10'' - 80''$) zone (3) the number in the outer ($> 80''$) background zone (4) the number in the inner zone corrected for completeness, and (5) the net GCLF, after subtraction of the area-normalized background counts.

To estimate the turnover level and shape of the GCLF, we fit a standard Gaussian interpolation function (Harris 1991; Jacoby et al. 1992) to the data shown in Fig. 10, setting the standard deviation σ_V of the curve and then solving for the best-fit turnover level V^0 . Trials with different adopted σ_V 's gave the results summarized in Table 5. The reduced $\tilde{\chi}^2$ values favor a solution in the broad range $\sigma_V \sim 1.4 - 1.8$, with little to choose among values in this range in a formal sense. However, it is well known that both σ_V and V^0 tend to be overestimated in situations like these where the magnitude limit of the data reaches barely past the actual turnover (e.g., Hanes & Whittaker 1987; Paper I) since the solutions for the two parameters are correlated. For this reason, we favor a choice in the narrower range $\sigma_V \simeq 1.4 - 1.6$ and $V^0 \simeq 27.6 - 28.0$. Sample Gaussian curves for the extremes of this range are shown in Fig. 10.

Our final adopted pair of parameters is $V^0 = 27.8 \pm 0.2$, $\sigma_V = 1.5 \pm 0.1$. For comparison,

Baum et al. (1997) found $V^0 = 27.72$ employing a different and more complex fitting function. As is discussed more extensively in Paper I, this turnover level is also similar to what we found in the central cD NGC 4874. Using both of them combined, along with a calibration of the absolute magnitude of the turnover point based on the Virgo ellipticals, we find $d \sim 100$ Mpc for Coma along with a Hubble constant $H_0 \simeq 70$ (see Paper I).

A second and more physically oriented way to display the same material is as the *luminosity distribution function* (LDF), or number of clusters per unit (linear) luminosity. (The relation between the GCLF and LDF forms is exhaustively discussed by McLaughlin 1994.) The LDF is shown in Figure 11. At levels brighter than the GCLF “turnover” (which in turn is only slightly brighter than the photometric completeness limit), the LDF clearly approximates a power-law falloff toward higher luminosity, $N(L)dL \sim L^{-\alpha}$. To second order, however, the slope $\alpha = -d\log(N)/d\log(L)$ appears to steepen slightly at the upper end: an unweighted least-squares fit to all bins brighter than the turnover yields $\alpha = 2.05$, while exclusion of the half-dozen very brightest bins yields $\alpha = 1.75$.

These power-law forms – as well as logarithmic slope values $\alpha \sim 2$ – are entirely similar to what has been found in a wide range of other galaxies from dwarf ellipticals to spirals (Harris & Pudritz 1994; Durrell et al. 1996). However, in most giant ellipticals studied to date, the slopes tend to be somewhat flatter at $\alpha \sim 1.5 \pm 0.3$ (Harris & Pudritz 1994). The total shape for $\log(L/L_\odot) \gtrsim 5$, complete with its progressive steepening toward higher luminosity, can be well matched by a formation model in which protocluster clouds build up by collisional agglomeration and in which the more massive clouds have shorter lifetimes against star formation (McLaughlin & Pudritz 1996; Harris 2000). Our data for IC 4051 add further to the general body of material which indicates a remarkable place-to-place similarity in the luminosities of old globular clusters, and thus a quasi-universal formation process.

5. RADIAL DISTRIBUTION AND SPECIFIC FREQUENCY

Because the GCS around IC 4051 is quite centrally concentrated (see Fig. 8), we can use the complete WFPC2 data to define the spatial distribution outward nearly to its limits. The radial profile of the raw counts for all starlike objects brighter than $V = 27.0$, for which the data are highly complete nearly in to the central core of the galaxy, is shown in Figure 12. The inner core ($R \lesssim 5''$), in which the projected density of clusters is nearly flat, continues outward to a steep power-law falloff which covers most of our survey area. Finally, for $R > 80''$, the number density σ begins to level off towards its eventual far-field background level; more or less arbitrarily, we set this background at $\sigma_b = (0.02 \pm 0.01)$

arcsec⁻² as representing nearly the average of the outermost two points. (As will be seen below, small differences in the adopted σ_b will not have major effects on any of our subsequent conclusions.)

The complete profile data broken into circular annuli are listed in Table 6, giving the number of objects in each bin, the surface area of the annulus, and the projected density σ . The residual number density of clusters, $\sigma_{cl} = \sigma - \sigma_b$, is plotted in Figure 13. Simple King (1966) models can be fitted to the σ_{cl} data points to give rough estimates of the GCS core radius and central concentration: performing a weighted fit in the manner described in Paper II, and ignoring the very uncertain outermost three points, we find a formal best-fit core radius $R_c = 10''.25$ (equivalent to 5.1 kpc at the adopted Coma distance) as well as a concentration index $c = 1.45$ for a dimensionless central potential $W_0 = 6.26$. The core radius is four times smaller in IC 4051 than the ~ 22 kpc value we found in the much more extended NGC 4874 (Paper II).

A second comparison can be made with the halo *light* of the galaxy. It is conventionally found in giant ellipticals that the GCS is a more spatially extended system as a whole than the halo (Harris 1991, 1999). IC 4051 is no exception, despite its overall compact structure. In Fig. 13, we show the wide-field surface intensity profiles in μ_R measured by Strom & Strom (1978) and Jorgensen et al. (1992). Although the Strom data are photographically measured, their profile agrees tolerably with the more recent CCD measurements of Jorgensen et al. (1992) over their region of overlap.

The bulk of the GCS profile is more extended than the halo light, except possibly for the outer ($R \gtrsim 30''$) regions where their slopes are more nearly similar. For $R \gtrsim 20''$, the GCS profile behaves as $\sigma_{cl} \sim R^{-2}$, although at the largest radii little weight can be placed on the very uncertain outermost half-dozen points. There is a strong hint from the halo light profile that the galaxy may be truncated past $R \sim 60''$ (about 30 kpc), though here again the profile is very sensitive to slight differences in the adopted background level, so not much meaning can be ascribed to the slope differences between the GCS and the halo there. For giant E galaxies in general, a rough mean relation between galaxy luminosity M_V^T and the radial falloff outside the central core is (Kaisler et al. 1996) $d\log\sigma/d\log R \simeq -0.29M_V^T - 8.00$. For IC 4051, this relation would predict $\sigma_{cl} \sim R^{-1.65}$, somewhat flatter than the observed R^{-2} trend.

Calculating the total GCS population and specific frequency is now a straightforward matter. From Table 6, we multiply $\sigma_{cl}(R)$ by the area of each annulus, then sum the annuli to get the total cluster population out to the limits of our survey. We find $N = (1845 \pm 165)$ for $V \leq 27.0$ and $R \lesssim 130''$. If the true GCLF turnover magnitude is at $V^0 = 27.8 \pm 0.2$ (see above), then we must multiply this raw total by $\simeq (3.35 \pm 0.52)$ to estimate the total cluster

population over all magnitudes, giving $N_{cl} = 6180 \pm 1100$. The integrated luminosity of the galaxy is $V^T = 13.20$ (RC3 catalog value), corresponding to $M_V^T = -21.9$ for our adopted Coma distance. Thus, the specific frequency is

$$S_N = N_{cl} \cdot 10^{0.4(M_V^T + 15)} = 10.8 \pm 1.9.$$

In strict terms this is a *lower limit* to the true global S_N , since we have not accounted for any cluster population outside the $\simeq 120''$ radial limit of our WFPC2 field. However, given that the halo is clearly declining quite steeply in this region (Fig. 13), any such population correction is likely to be small. A generous but reasonable *upper limit* estimate to the total population can be made if we assume that the GCS profile continues as $\sigma_{cl} \sim R^{-2}$ outward to the nominal tidal radius at $R_t \sim 230''$. This assumption gives an additional $\sim 380 \pm 300$ clusters brighter than $V = 27$, which then translates to $S_N = 12.6 \pm 2.6$.

Placing more weight on the lower limit – which reflects the steep falloff of the system near the radial limit of our data – we adopt a final estimate

$$S_N(\text{final}) = 11 \pm 2.$$

Remarkably, this GCS population ratio is several times higher than the $S_N \lesssim 2$ value found in NGC 4881 (Baum et al. 1995), a galaxy which is quite comparable with IC 4051 in luminosity, structure, and location on the outskirts of the Coma core. This high S_N , in fact, places IC 4051 in the range which is conventionally reserved for the central-giant cD galaxies like M87 and many other BCGs (Harris et al. 1998; Blakeslee 1997, 1999). It is, perhaps, particularly noteworthy that IC 4051 has a specific frequency three times higher than the central cD *in its own host galaxy cluster*, NGC 4874 (see Paper II). No other instance of such a large contrast between a low- S_N central cD and a higher- S_N outlying elliptical is known. IC 4051 provides striking evidence that a central location in a rich cluster environment is *not* required to form a high population of globular clusters.

6. DISCUSSION

A brief summary of our findings for IC 4051 is that its GCS is (a) almost entirely metal-rich, albeit possibly with two narrowly separated subcomponents; (b) relatively compact in radial structure; and (c) a “high specific frequency” system despite that fact that its host galaxy is not a central giant elliptical nor one with a cD-type envelope.

Just as in Paper II for NGC 4874, we now attempt to use the integrated characteristics to reconstruct a partial history of the system. Formation scenarios for giant ellipticals tend

to fall into three basic camps: (a) “in situ” formation, whereby the galaxy condenses by dissipative collapse of gas clouds in its immediate vicinity, in one or more major bursts; (b) later mergers of pre-existing disk-type galaxies with both gas and stars; or (c) successive mergers or accretions of smaller gas-poor satellites. Various combinations of these extremes are, of course, possible, and even likely.

For IC 4051, the lack of *low*-metallicity clusters already places fairly strong constraints on the range of possible formation events. For example, the mechanism investigated by Côté et al. (1998) – in which an original metal-rich “seed” gE accretes dozens or hundreds of smaller satellites – is unlikely, since these dwarf satellites would have brought in a population of hundreds or even thousands of low-metallicity clusters, which we do not see.

Similarly, merger-formation models in which gas-rich disk galaxies combine to build a composite elliptical (Ashman & Zepf 1992) would predict a strong component of metal-poor clusters in the resulting MDF from the globular clusters that were present in the pre-merger galaxies. These merger models also have severe difficulty in generating high specific frequency products, since increasing the cluster population *relative to the field stars* by a large enough amount to produce high S_N requires very large ($> 10^{10} M_\odot$) input gas masses, more than is routinely available in disk galaxies today. The normal merger route does appear to be quite effective as a logical source for low- S_N field ellipticals (see Harris 2000 or Whitmore & Schweizer 1995 for much more extensive discussion).

However, if either the merger or accretion processes are taken to an extreme form in which *the merging objects are almost completely gaseous*, then they become closely similar to the *in situ* route, and the conundrum of the missing low-metallicity clusters can be more easily circumvented. If the gas supply – however it was assembled – underwent most or all of its star formation in the high-pressure, high-density environment of the protoelliptical, then the conversion of gas to stars would have run much further to completion and built up the metallicity to the high levels that we now observe. Later gaseous mergers are, of course, not ruled out: the central corotating disk in the core of IC 4051 (Mehlert et al. 1998) with its very high metallicity is a likely signature of such an event, though at its $\lesssim 1\%$ contribution to the present-day luminosity, it probably did not form more than a few dozen globular clusters along with it, and even these would have mostly disrupted by now if they resided in the central few kpc of the core.

The relatively compact structure of the galaxy may be the result of tidal trimming (“harrassment”) from the Coma potential well (e.g., Moore et al. 1996). The radial velocity of IC 4051 (4940 km s^{-1}) is almost two standard deviations away from the Coma centroid (6850 km s^{-1} ; see Colless & Dunn 1996), indicating that this galaxy oscillates back and forth through the cluster and is now passing through the dense Coma core at high speed.

These elements of an evolutionary scenario for IC 4051 are in strong contrast to NGC 4874, for which we argued (Paper II) that a large fraction of its clusters (which are almost entirely low-metallicity) could have been acquired by accretions of smaller satellites. In IC 4051, we are forced to argue that the bulk of its clusters formed *in situ*. The globular clusters in these two galaxies provide unique evidence for the view that large E galaxies can form by radically different evolutionary routes.

One of the most challenging elements of IC 4051 to interpret is certainly the high specific frequency of its GCS. In the previous literature (Harris 1991, 2000; Blakeslee 1997, 1999; Harris et al. 1998; McLaughlin 1999) it has become conventional to associate high S_N with giant galaxies at the centers of rich clusters. These central BCG’s or cD’s can have had histories of star and cluster formation through inflowing gas clouds and filaments, mergers, and accretions (e.g., Dubinski 1998) that were much more extended than for normal outlying ellipticals. Recently, the view has been developed that such high- S_N galaxies should be regarded not as “cluster-rich” but rather as “star-poor” (Blakeslee 1997, 1999; Harris et al. 1998; McLaughlin 1999). In this scheme, we postulate that the protogalactic gas started forming globular clusters at early times at a normal efficiency rate, but was then disrupted (perhaps by supernova-driven galactic winds, or by tidal shredding during infall; cf. the papers cited above) before its star formation could run to completion. The leftover gas now remains around these galaxies as their hot X-ray halos. This picture, however, assumes that the globular clusters form earlier than the bulk of the field stars in any given round of star formation – not an implausible requirement given the bulk of the observational evidence for starburst systems (see Harris 2000) and given that globular clusters emerge from the densest, most massive protocluster clouds.

McLaughlin (1999) defines a globular cluster formation efficiency, measured empirically as the mass ratio

$$\epsilon = \frac{M_{cl}}{M_{\star} + M_{gas}}$$

where M_{\star} and M_{gas} are the masses within the galaxy in the form of visible stars and in the X-ray gas respectively. He finds that ϵ is essentially identical in the well studied Virgo and Fornax systems M87, NGC 4472, and NGC 1399 (despite their very different S_N), providing evidence for a “universal” globular cluster formation efficiency $\epsilon \simeq 0.26\%$ relative to the *initial protogalactic gas supply*. The total mass ratio ϵ is a more important indicator of cluster formation than S_N , which is only a measure of the cluster numbers (or equivalently total mass) relative to the galaxy light. In other words, S_N is a measure of only the gas mass M_{\star} that got converted to stars. Additional support for the near-universality of ϵ in several other BCG’s is found by Blakeslee (1999) .

In this view, *any high- S_N galaxy should then be surrounded by a massive X-ray gaseous*

component whether or not it is a centrally dominant giant. Notably, IC 4051 is indeed one of the few Coma ellipticals with an individually detected X-ray halo. Dow & White (1995), from ROSAT observations of the Coma core region, find that IC 4051 is detectable at the $2 - \sigma$ level in the soft X-ray range $0.2 - 0.4$ keV, but not in the higher $0.4 - 2.4$ keV range. If it were at the ~ 6.3 times closer distance of Virgo, IC 4051 would have a total $L_X \simeq 5 \times 10^{41}$ erg s $^{-1}$. This level makes it quite comparable with the Virgo giant NGC 4472, which has $L_X \simeq 6 \times 10^{41}$ erg s $^{-1}$ in the soft X-ray regime (Fabbiano et al. 1992; Irwin & Sarazin 1996; Matsumoto et al. 1997; Buote & Fabian 1998). However, this amount of X-ray gas corresponds to only $\sim 5\%$ of the stellar mass (McLaughlin 1999) and NGC 4472, as expected, has only a “normal” specific frequency level $S_N \simeq 5$.

With our adopted distance ratios for Virgo and Coma, we find that IC 4051 is about half as luminous as NGC 4472, so if it has a roughly similar amount of X-ray gas mass, this gas would only make up $\sim 10\%$ of its stellar mass. Along with $S_N \simeq 11$, we find that these parameters convert to a *present-day* value for the mass ratio in IC 4051 of $\epsilon \sim 0.005$, twice as large as McLaughlin’s (1999) fiducial value.

Nominally, it therefore seems that IC 4051 acts against the paradigm of a universal globular cluster formation efficiency. An obvious possibility, however, is that IC 4051 originally did possess much more gas shortly after its main era of globular cluster formation, but that most of this unused material was quickly stripped away as IC 4051 went through its first few passages of the Coma core. This gas would have joined the general reservoir of hot gas spread throughout the Coma potential well. The same mechanism which resulted in this galaxy’s compact structure might then have plausibly left it with the unusual combination of high S_N and modest amount of X-ray gas that we now see.

A situation which would act much more strongly to falsify McLaughlin’s case for a universal ϵ would be the opposite one: that is, a galaxy with a massive X-ray halo but a “normal” or subnormal $S_N \lesssim 4$. In such a case it would be much harder to avoid the conclusion that the formation efficiency of globular clusters was genuinely different (and low). Does the central Coma giant NGC 4874 present us with such a case? As we found in Paper II, NGC 4874 is *not* a high- S_N system and is embedded within a very massive X-ray envelope. This X-ray gas is, however, so extended that must belong to the general Coma potential well as a whole, with no detectable concentrated component that can be associated with NGC 4874 itself (Dow & White 1995). Thus there are ambiguities in the interpretation that are hard to circumvent. Better candidates would be E galaxies with massive X-ray halos that are not at the centers of rich clusters.

Finally, we may compare the interesting case of IC 4051 with that of its Coma neighbor NGC 4881 (Baum et al. 1995), a giant E galaxy of similar location, size, and structure.

Curiously, NGC 4881 holds a GCS of *low* specific frequency ($S_N \lesssim 2$) which appears to be almost entirely metal-*poor*, just the opposite of IC 4051. It has no significant amounts of X-ray gas (Dow & White 1995). We speculate that NGC 4881 may have resulted from the merger of smaller galaxies in which these metal-poor globulars had already formed. These mergers should have been rather gas-poor to prevent the formation of newer and more metal-rich clusters. This is, however, an extremely sketchy interpretation, and there is an obvious problem with the much higher metallicity of the host galaxy light (how did the bulk of the giant E galaxy form at higher metallicity without leaving behind some metal-rich globular clusters? See Paper II for additional discussion).

The Coma ellipticals clearly present a wide range of GCS characteristics that strongly challenge the array of current galaxy formation models.

This research was supported through a grant to WEH from the Natural Sciences and Engineering Research Council of Canada. We thank Peter Macdonald of Ichthus Data Systems and the Department of Mathematics and Statistics at McMaster for providing the MIX multicomponent fitting code. Bill Baum provided several constructive comments on the first version of the text.

REFERENCES

- Armandroff, T. E., & Zinn, R. 1988, AJ, 96, 92
- Ashman, K. M., & Zepf, S. E. 1992, ApJ, 384, 50
- Baum, W. A. et al. 1995, AJ, 110, 2537
- Baum, W. A. et al. 1997, AJ, 113, 1483
- Blakeslee, J. P. 1997, ApJ, 481, L59 (B97)
- Blakeslee, J. P. 1999, AJ, 118, 1506
- Buote, D. A., & Fabian, A. C. 1998, MNRAS, 296, 977
- Buta, R., & Williams, K. L. 1995, AJ, 109, 543
- Colless, M., & Dunn, A. M. 1996, ApJ, 458, 435
- Côté, P., Marzke, R., & West, M. J. 1998, ApJ, 501, 554
- Dow, K. L., & White, S. D. M. 1995, ApJ, 439, 113
- Dubinski, J. 1998, ApJ, 502, 141
- Durrell, P. R., Harris, W. E., Geisler, D., & Pudritz, R. E. 1996, AJ, 112, 972
- Fabbiano, G., Kim, D.-W., & Trinchieri, G. 1992, ApJS, 80, 531
- Geisler, D., Lee, M. G., & Kim, E. 1996, AJ, 111, 1529
- Hanes, D. A., & Whittaker, D. G. 1987, AJ, 94, 906
- Harris, W. E. 1991, ARA&A, 29, 543
- Harris, W. E. 1996, AJ, 112, 1487
- Harris, W. E. 2000, Lectures for 1998 Saas-Fee Advanced School on Star Clusters, in press
- Harris, W. E., Allwright, J. W. B., Pritchett, C. J., & van den Bergh, S. 1991, ApJS, 76, 115
- Harris, W. E., Harris, G. L. H., & McLaughlin, D. E. 1998, AJ, 115, 1801
- Harris, W. E., Kavelaars, J. J., Hanes, D. A., Hesser, J. E., & Pritchett, C. J. 2000, ApJ, 533, in press (Paper II)

- Harris, W. E., & Pudritz, R. E. 1994, *ApJ*, 429, 177
- Holtzman, J. A. et al. 1995, *PASP*, 107, 1065
- Irwin, J. A., & Sarazin, C. 1996, *ApJ*, 471, 683
- Jacoby, G. H. et al. 1992, *PASP*, 104, 599
- Jorgensen, I., Franx, M., & Kjaergaard, P. 1992, *AApS*, 95, 489
- Kaisler, D., Harris, W. E., Crabtree, D. R., & Richer, H. B. 1996, *AJ*, 111, 2224
- Kavelaars, J. J., Harris, W. E., Hanes, D. A., Hesser, J. E., & Pritchett, C. J. 2000, *ApJ*, 533, in press (Paper I)
- King, I. R. 1966, *AJ*, 71, 64
- Kundu, A., & Whitmore, B. C. 1999, *Bull.AAS*, 31, 874
- Kundu, A., Whitmore, B. C., Sparks, W. B., Macchetto, F. D., Zepf, S. E., & Ashman, K. M. 1999, *ApJ*, 513, 733
- Lee, M. G., Kim, E., & Geisler, D. 1998, *AJ*, 115, 947
- Matsumoto, H., Koyama, K., Awaki, H., & Tsuru, T. 1997, *ApJ*, 482, 133
- McLaughlin, D. E. 1994, *PASP*, 106, 47
- McLaughlin, D. E. 1999, *AJ*, 117, 2398
- McLaughlin, D. E., & Pudritz, R. E. 1996, *ApJ*, 457, 578
- Mehlert, D., Saglia, R. P., Bender, R., & Wegner, G. 1998, *A&A*, 332, 33
- Moore, B., Katz, N., Lake, G., Dressler, A., & Oemler, A. Jr 1996, *Nature*, 379, 613
- Neilsen, E. H., & Tsvetanov, Z. I. 1999, *ApJ*, 515, L13
- Ostrov, P., & Forte, J. C. 1998, *AJ*, 116, 2854
- Prugniel, Ph., & Héraudeau, Ph. 1998, *AApS*, 128, 299
- Secker, J., Geisler, D., McLaughlin, D. E., & Harris, W. E. 1995, *AJ*, 109, 1019
- Stetson, P. B. 1992, in *Astronomical Data Analysis Software and Systems I*, ASP Conf. Ser. 8, edited by G. H. Jacoby (ASP, San Francisco), p. 289

Strom, K. M., & Strom, S. E. 1978, AJ, 83, 73

Whitmore, B. C., & Schweizer, F. 1995, AJ, 109, 960

Whitmore, B. C., Sparks, W. B., Lucas, R. A., Macchetto, F. D., & Biretta, J. A. 1995,
ApJ, 454, L73

Zinn, R. 1985, ApJ, 293, 424

Table 1. Completeness Function Parameters

CCD	$F606W(V)$		$F814W(I)$	
	α	V_{lim}	α	I_{lim}
PC1	3.508	27.85	3.682	25.70
WF2	3.141	28.39	3.078	26.13
WF3	3.123	28.46	3.157	26.24
WF4	3.154	28.39	3.530	26.18

Table 2. Mean Color vs. V Magnitude

V	N	$\langle V - I \rangle$	$\sigma_{(V-I)}$
22.5–23.0	7	1.058	0.031
23.0–23.5	7	1.136	0.053
23.5–24.0	20	1.101	0.018
24.0–24.5	43	1.111	0.016
24.5–25.0	77	1.128	0.012
25.0–25.5	145	1.113	0.010
25.5–26.0	180	1.119	0.010

Table 3. Mean Color vs. Radius

R (arcsec)	N	$\langle V - I \rangle$	\pm	$\langle \text{Fe}/\text{H} \rangle$	\pm
0.0– 8.0	79	1.170	0.013	+0.04	0.08
8.0–12.0	80	1.141	0.011	–0.14	0.07
12.0–16.0	61	1.116	0.014	–0.28	0.08
16.0–26.0	68	1.083	0.015	–0.48	0.09
26.0–40.0	75	1.120	0.013	–0.26	0.08
40.0–55.0	51	1.120	0.017	–0.26	0.10
55.0–80.0	65	1.050	0.015	–0.67	0.09

Table 4. Binned GCLF Data

V	N_{in}	N_{out}	$N_{in,corr}$	N_{final}
22.1–22.4	1.0 ± 1.0	0.0 ± 0.0	1.0 ± 1.0	1.0 ± 1.0
22.4–22.7	1.0 ± 1.0	1.0 ± 1.0	1.0 ± 1.0	-0.9 ± 1.5
22.7–23.0	5.0 ± 2.2	1.0 ± 1.0	5.0 ± 2.2	3.1 ± 2.5
23.0–23.3	1.0 ± 1.0	0.0 ± 0.0	1.0 ± 1.0	1.0 ± 1.0
23.3–23.6	7.0 ± 2.6	2.0 ± 1.4	7.0 ± 2.6	3.1 ± 3.0
23.6–23.9	13.0 ± 3.6	1.0 ± 1.0	13.0 ± 3.6	11.1 ± 3.8
23.9–24.2	11.0 ± 3.3	1.0 ± 1.0	11.0 ± 3.3	9.1 ± 3.5
24.2–24.5	22.0 ± 4.7	2.0 ± 1.4	22.0 ± 4.7	18.2 ± 4.9
24.5–24.8	36.0 ± 6.0	2.0 ± 1.4	36.1 ± 6.0	32.2 ± 6.2
24.8–25.1	53.0 ± 7.3	1.0 ± 1.0	53.1 ± 7.3	51.2 ± 7.4
25.1–25.4	81.0 ± 9.0	7.0 ± 2.6	81.2 ± 9.0	67.7 ± 9.5
25.4–25.7	115.0 ± 10.7	12.0 ± 3.5	115.4 ± 10.8	92.2 ± 11.4
25.7–26.0	108.0 ± 10.4	17.0 ± 4.1	108.5 ± 10.4	75.5 ± 11.3
26.0–26.3	159.0 ± 12.6	23.0 ± 4.8	159.9 ± 12.7	115.3 ± 13.7
26.3–26.6	229.0 ± 15.1	43.0 ± 6.6	230.8 ± 15.3	147.4 ± 16.8
26.6–26.9	263.0 ± 16.2	44.0 ± 6.6	266.2 ± 16.4	180.5 ± 17.9
26.9–27.2	320.0 ± 17.9	42.0 ± 6.5	326.1 ± 18.2	244.1 ± 19.5
27.2–27.5	312.0 ± 17.7	66.0 ± 8.1	324.2 ± 18.4	194.2 ± 20.4
27.5–27.8	305.0 ± 17.5	57.0 ± 7.5	343.4 ± 19.9	229.0 ± 21.6
27.8–28.1	292.0 ± 17.1	66.0 ± 8.1	408.8 ± 27.5	268.0 ± 29.1
28.1–28.4	220.0 ± 14.8	81.0 ± 9.0	436.7 ± 44.0	216.9 ± 46.1
28.4–28.7	150.0 ± 12.2	66.0 ± 8.1	690.7 ± 87.7	291.9 ± 92.2
28.7–29.0	97.0 ± 9.8	46.0 ± 6.8	1076.5 ± 131.4	363.7 ± 144.4
29.0–29.3	8.0 ± 2.8	3.0 ± 1.7	159.9 ± 57.2	45.9 ± 68.4

Table 5. GCLF $\tilde{\chi}^2$ Fitting Results

σ_V	$\tilde{\chi}^2$	V_0
1.3	2.17	27.44
1.4	1.62	27.59
1.5	1.37	27.77
1.6	1.32	27.97
1.7	1.42	28.21
1.8	1.62	28.46

Table 6. Radial Density Profile

R (arcsec)	N	A (arcsec ²)	$\sigma(\text{n/arcsec}^2)$
0.0–2.0	16	12.533	1.277 ± 0.319
2.0–4.0	56	37.687	1.486 ± 0.199
4.0–6.0	86	62.845	1.368 ± 0.148
6.0–8.0	107	87.989	1.216 ± 0.118
8.0–10.0	113	113.069	0.999 ± 0.094
10.0–15.0	268	392.731	0.682 ± 0.042
15.0–20.0	172	442.020	0.389 ± 0.030
20.0–25.0	98	373.326	0.263 ± 0.027
25.0–30.0	91	459.581	0.198 ± 0.021
30.0–35.0	92	582.352	0.158 ± 0.017
35.0–40.0	68	702.702	0.097 ± 0.012
40.0–50.0	146	1762.469	0.083 ± 0.007
50.0–60.0	104	2235.922	0.047 ± 0.005
60.0–70.0	90	2431.022	0.037 ± 0.004
70.0–80.0	88	2484.612	0.035 ± 0.004
80.0–90.0	81	2594.925	0.031 ± 0.004
90.0–100.0	57	2124.154	0.027 ± 0.004
100.0–110.0	23	898.649	0.026 ± 0.005
110.0–130.0	9	521.199	0.017 ± 0.006

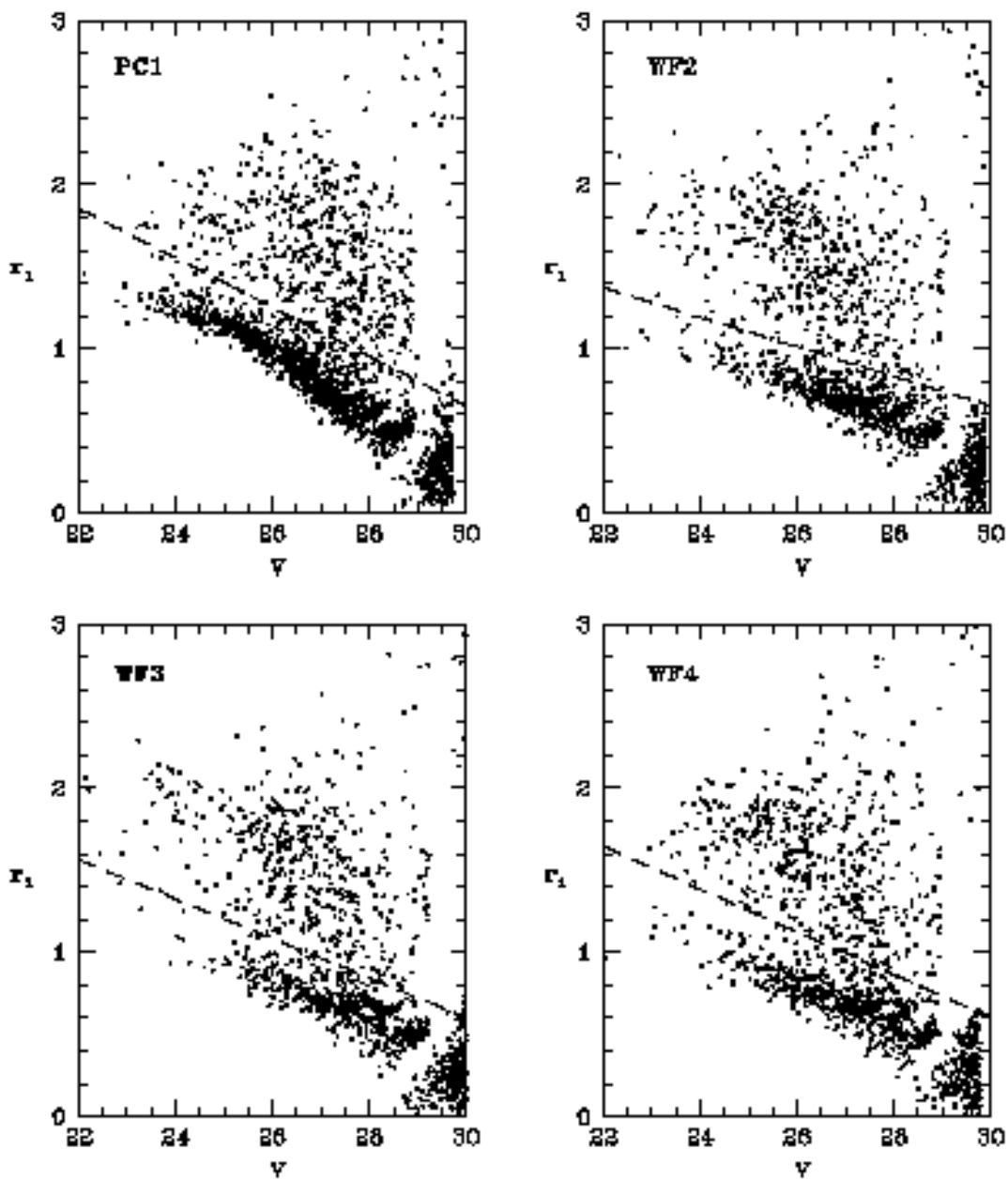


Fig. 1.— Image classification plots for all detected objects on the deep V exposures. The radial image moment r_1 (see text) is plotted against V for each of the four WFPC2 CCDs. The dashed lines show the adopted boundaries separating star-like objects (below the line) from nonstellar ones (above). The vast majority of the starlike objects are globular clusters around IC 4051.

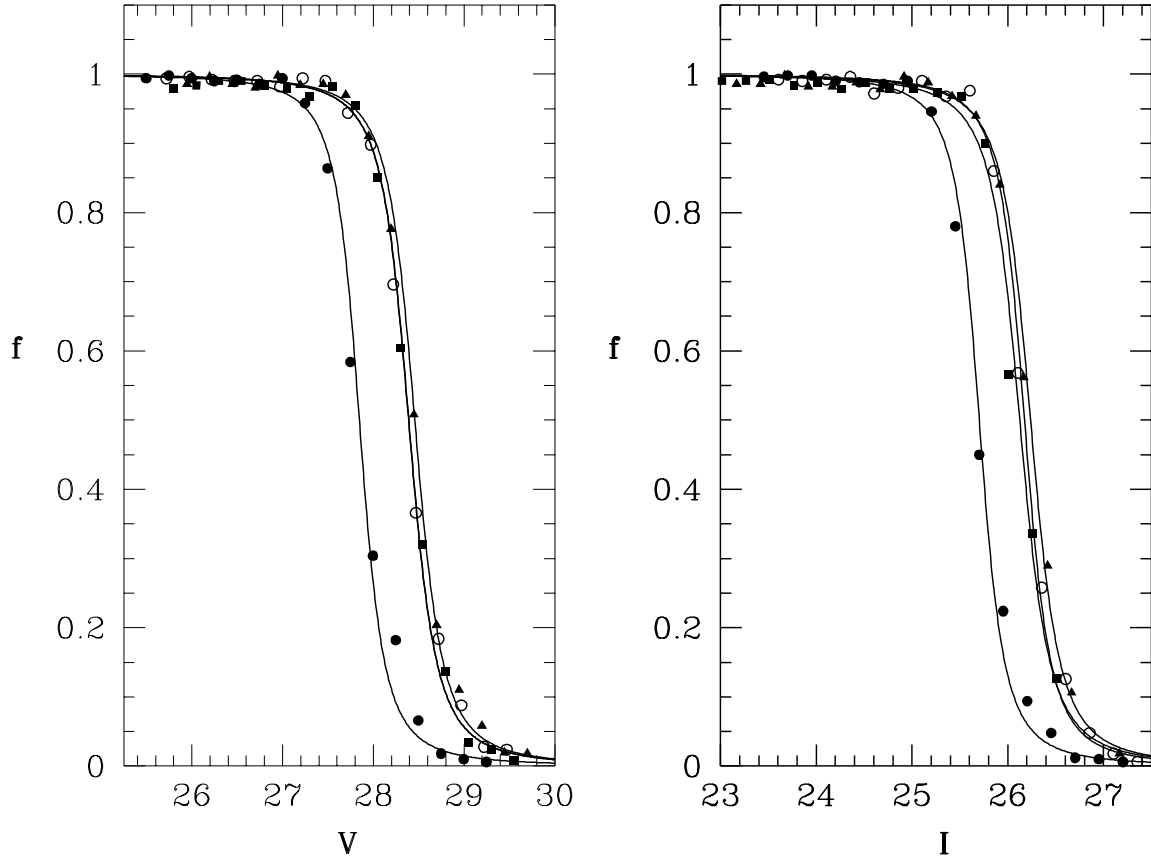


Fig. 2.— Completeness functions for the V (F606W) and I (F814W) photometry. The solid dots (leftmost curve) represent the PC1 data, solid squares represent WF2, solid triangles WF3, and open circles WF4. The lines through each set of points show the Pritchett interpolation function curves described in the text and parametrized in Table 1. The PC1 photometry has a noticeably brighter limiting magnitude.

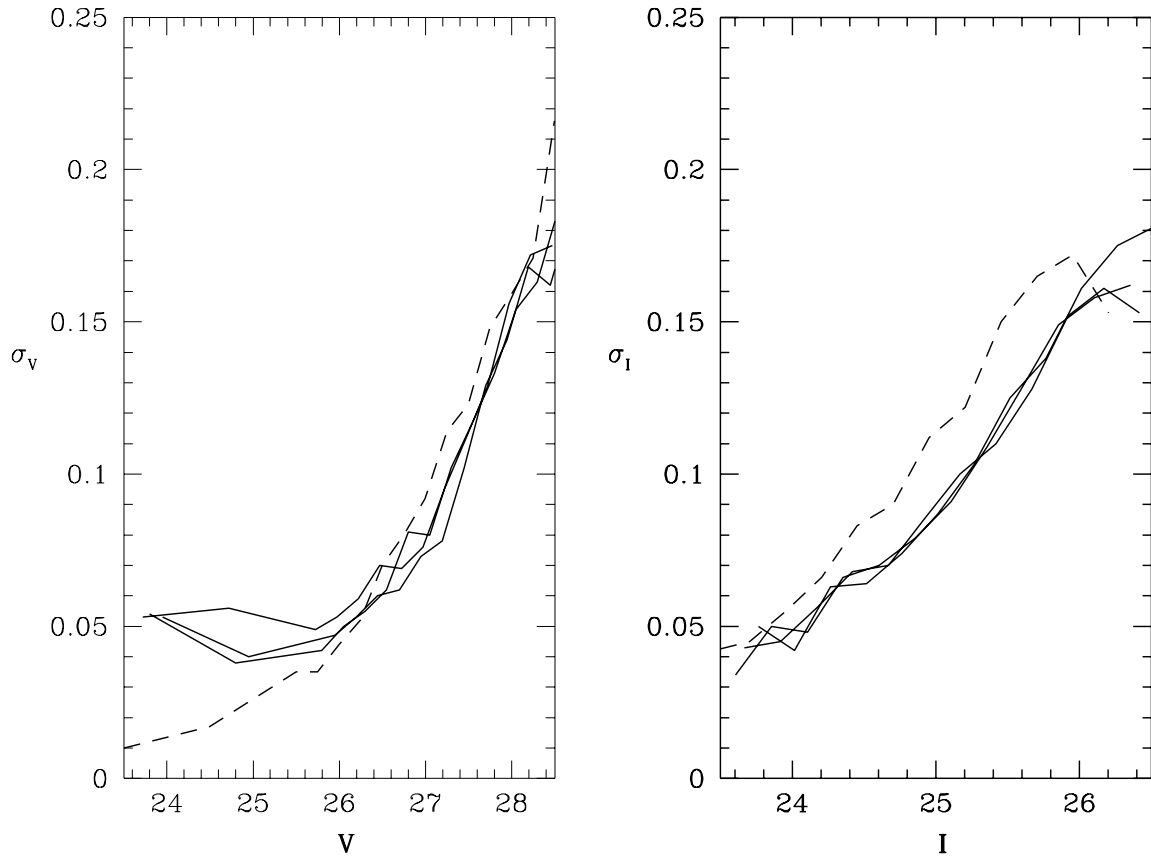


Fig. 3.— Mean photometric uncertainty as a function of magnitude, derived from the artificial-star tests. The dashed line represents the PC1, while the solid lines are for the WF2,3,4 chips. Here and in the completeness functions, there are no significant differences among the three WF chips.

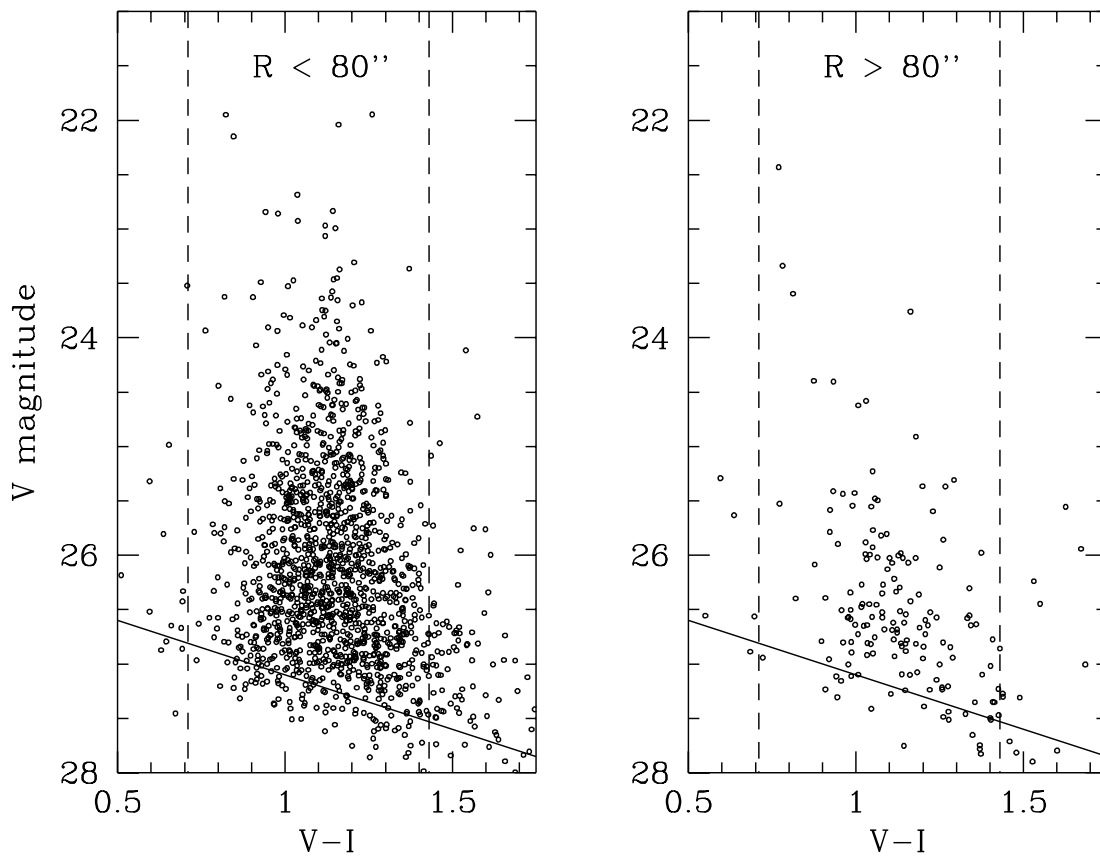


Fig. 4.— Color-magnitude distribution for all measured starlike objects with $(V - I)$ colors. The vast majority of these are globular clusters in IC 4051. Objects within $80''$ of the center of IC 4051 are plotted in the left panel, and objects lying beyond $80''$ in the right panel. The solid line shows the 50% detection completeness limit in I .

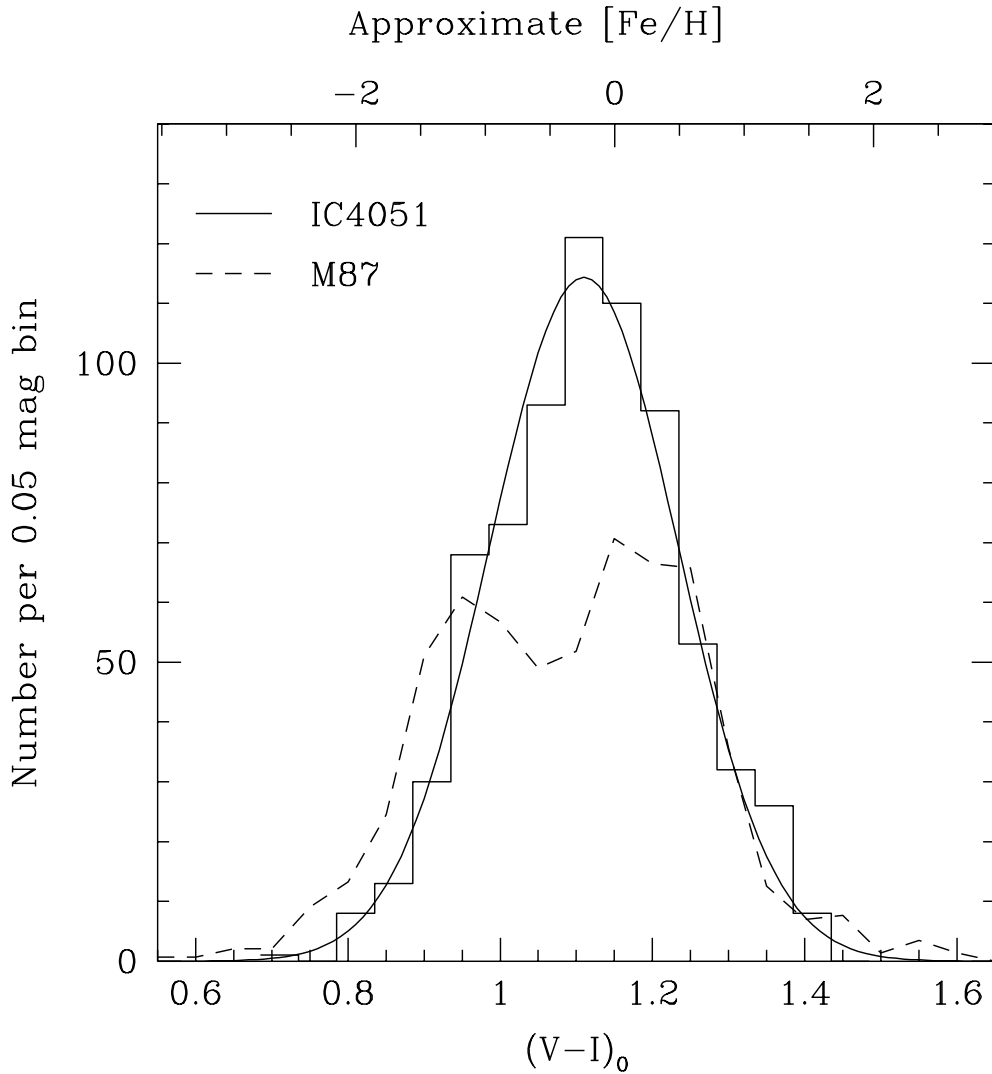


Fig. 5.— The metallicity distribution function (MDF) for the globular cluster system in IC 4051. Number of objects per 0.05-mag bin, after subtraction of background (see text), is plotted against $(V - I)$. The $[\text{Fe}/\text{H}]$ scale at top follows the linear conversion relation given in the text, and should be taken only as schematic for $[\text{Fe}/\text{H}] \gtrsim 0$. The best-fit single Gaussian function is shown, with $\langle V - I \rangle = 1.12$ and $\sigma(V - I) = 0.13$. The *dashed line* shows the color distribution for the globular clusters in the Virgo giant M87 (Kundu et al. 1999).

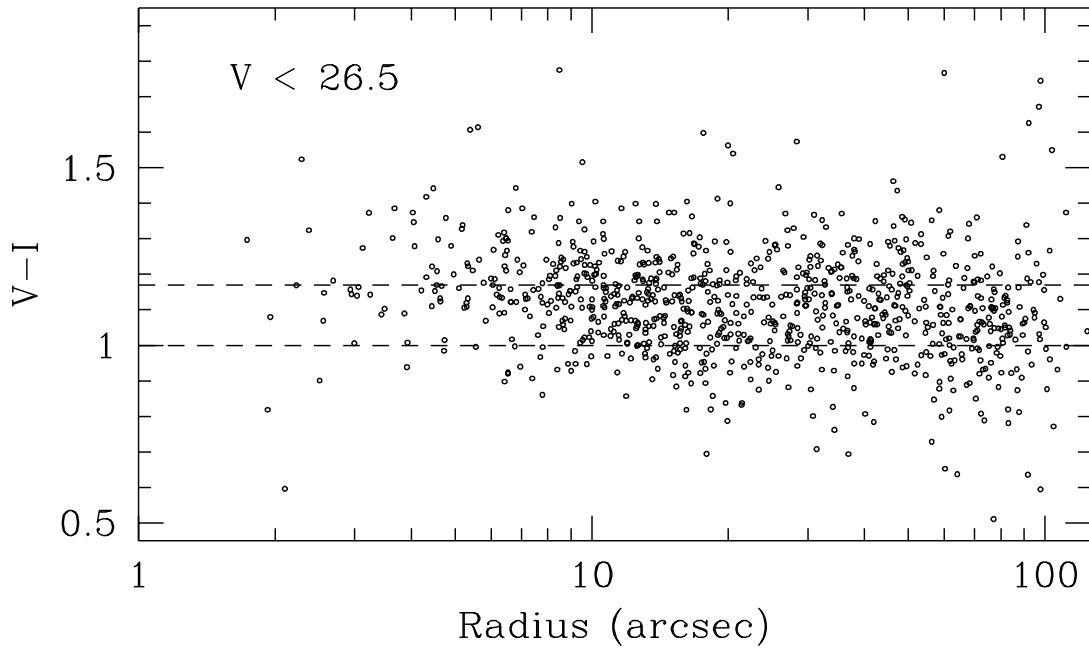


Fig. 6.— $V - I$ colour plotted against projected galactocentric distance, for bright objects ($V < 26.0$) for which the photometry is highly complete at all radii and the measurement uncertainties are smallest. Horizontal lines at $(V - I) = 1.17, 1.00$ are drawn at the suggested two subpopulations; the bluer of the two components is almost absent within $10''$.

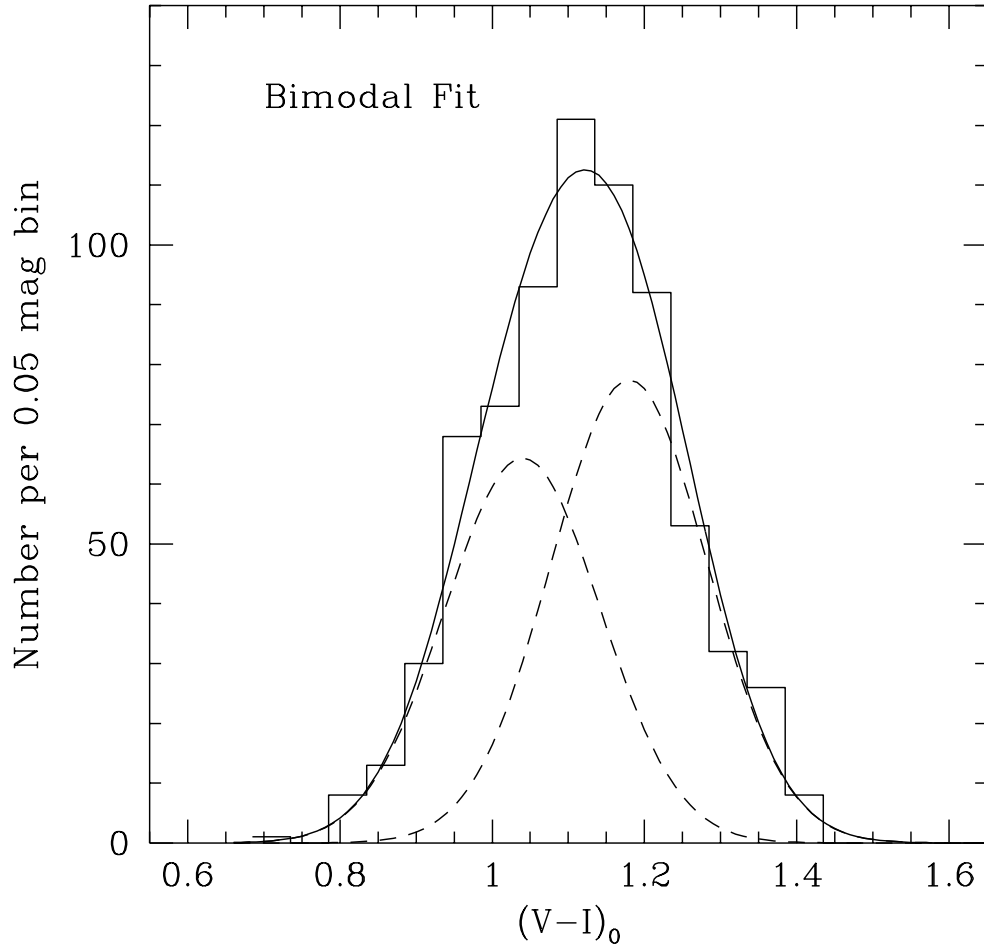


Fig. 7.— The color distribution of the clusters, fitted by a two-component Gaussian model as described in the text. The two subcomponents, centered at $(V - I) = 1.00, 1.17$ and each with $\sigma = 0.10$, are shown as the dashed lines, and their sum as the smooth solid line.

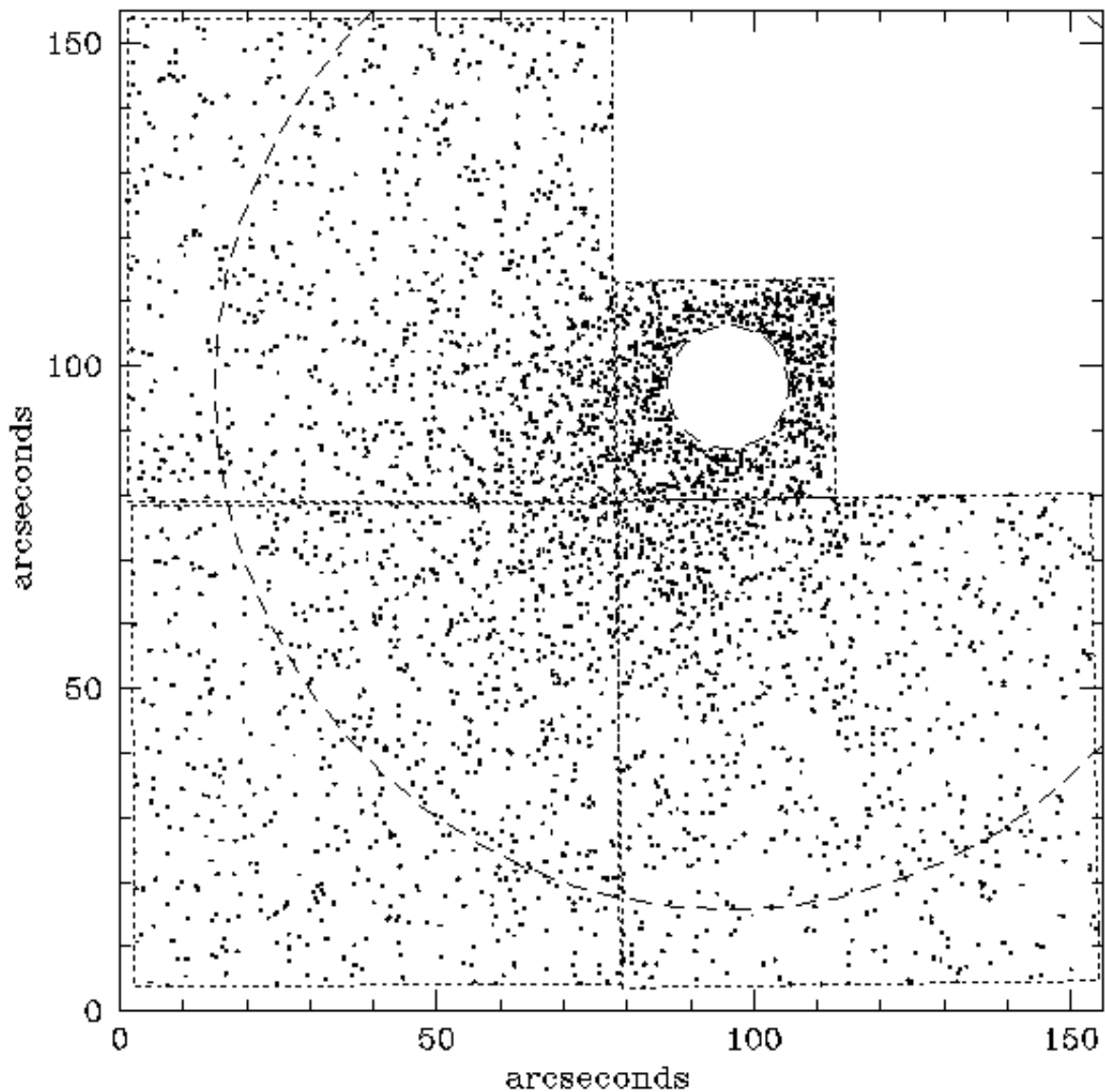


Fig. 8.— Spatial distribution of the globular clusters used to define the GCLF. Dotted lines outline the boundaries of the four CCDs. The zone outside the outer dashed circle at $R = 80''$ is used to define the “background” number density of objects. No data within $R = 10''$ (inner dashed circle) were used for the GCLF analysis. Note the obvious high concentration of the GC population toward the center of IC 4051.

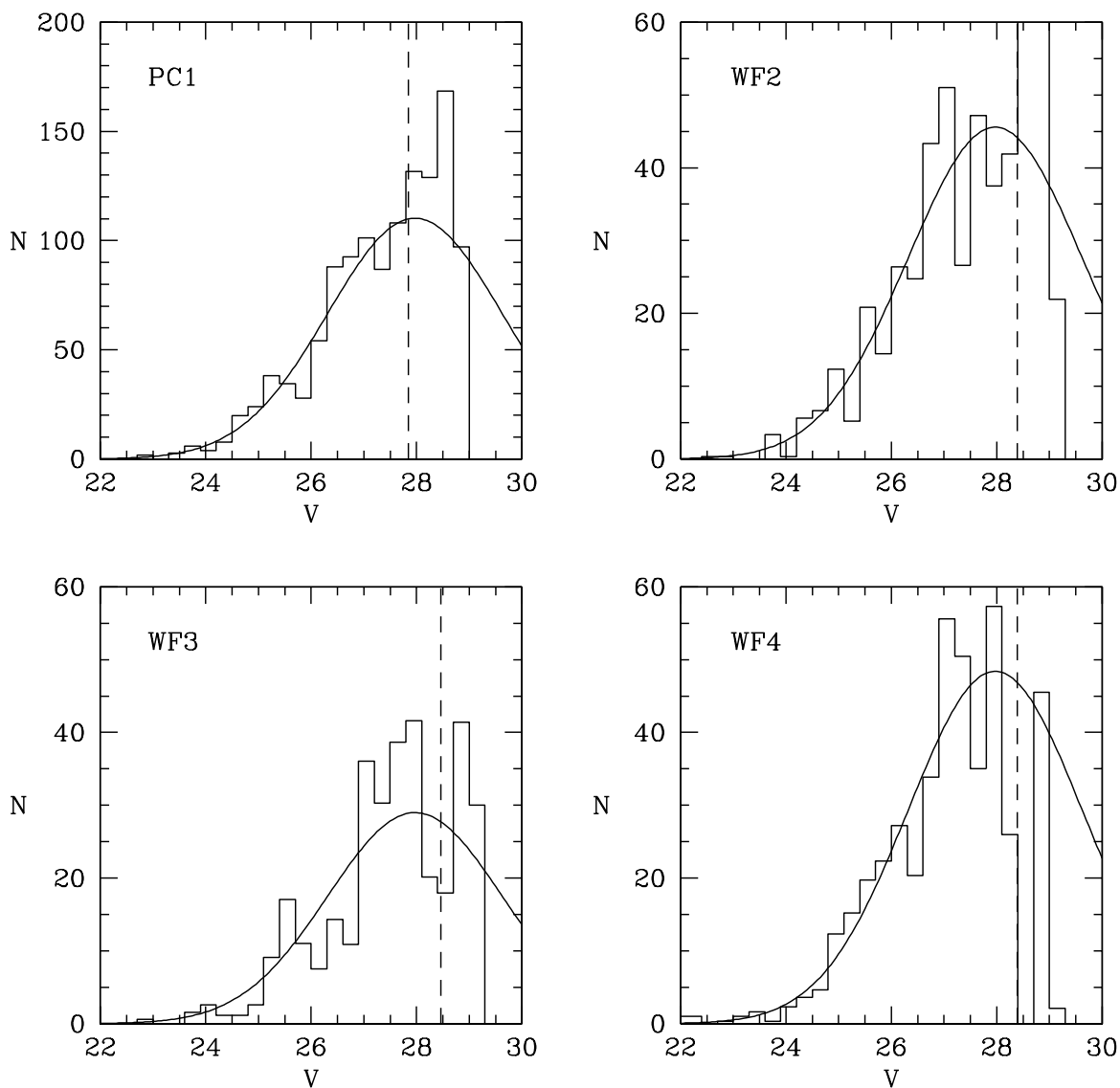


Fig. 9.— GCLFs (number of objects per 0.3-mag bin, after correction for incompleteness and subtraction of background) for the four separate WFPC2 chips. The dashed line in each graph represents the 50% completeness limit of the photometry, while the solid line shows the best-fit Gaussian function (see next Figure).

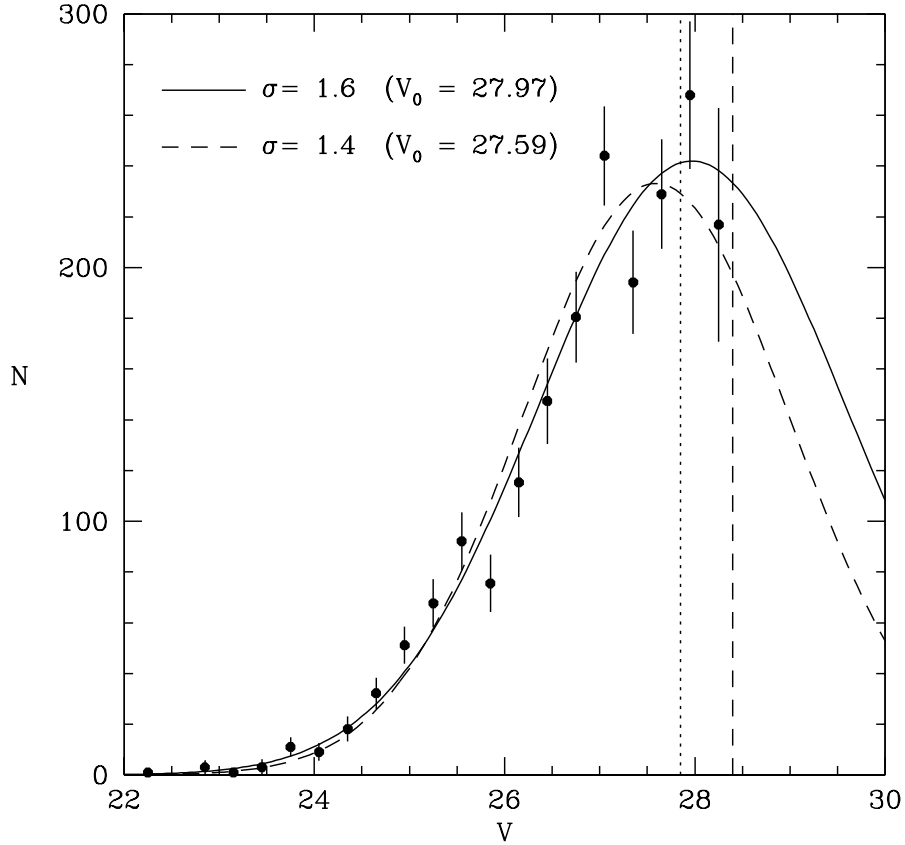


Fig. 10.— The GCLF for all combined V data (the sum of the four plots in the previous figure). The dotted and dashed vertical lines represent the 50% completeness limit of the PC1 and WF data respectively. The solid line is the best-fit Gaussian function to the binned data for an assumed GCLF dispersion $\sigma_V = 1.6$, while the dashed line is the best-fit Gaussian for $\sigma_V = 1.4$.

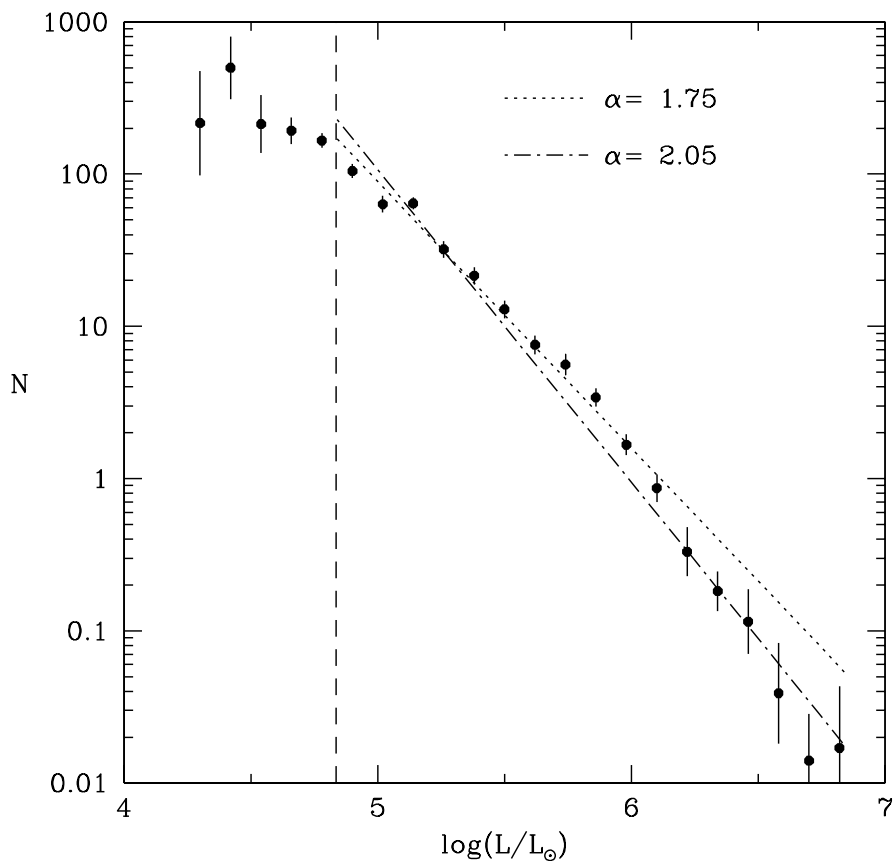


Fig. 11.— The luminosity distribution function (LDF, or number of clusters per unit luminosity L/L_{\odot}). The vertical dashed line shows the luminosity at which the GCLF (from the previous figure) reaches its peak or “turnover”, equivalent to $\log(L/L_{\odot}) \sim 4.8$. The dotted line is a weighted best-fit power-law function $N \sim L^{-\alpha}$ for the restricted range $4.8 \lesssim \log(L/L_{\odot}) \lesssim 6.5$, yielding $\alpha = 1.75$. An unweighted fit to all the data (dot-dashed line) yields a somewhat steeper slope $\alpha \simeq 2.05$ affected by the downturn at the bright end.

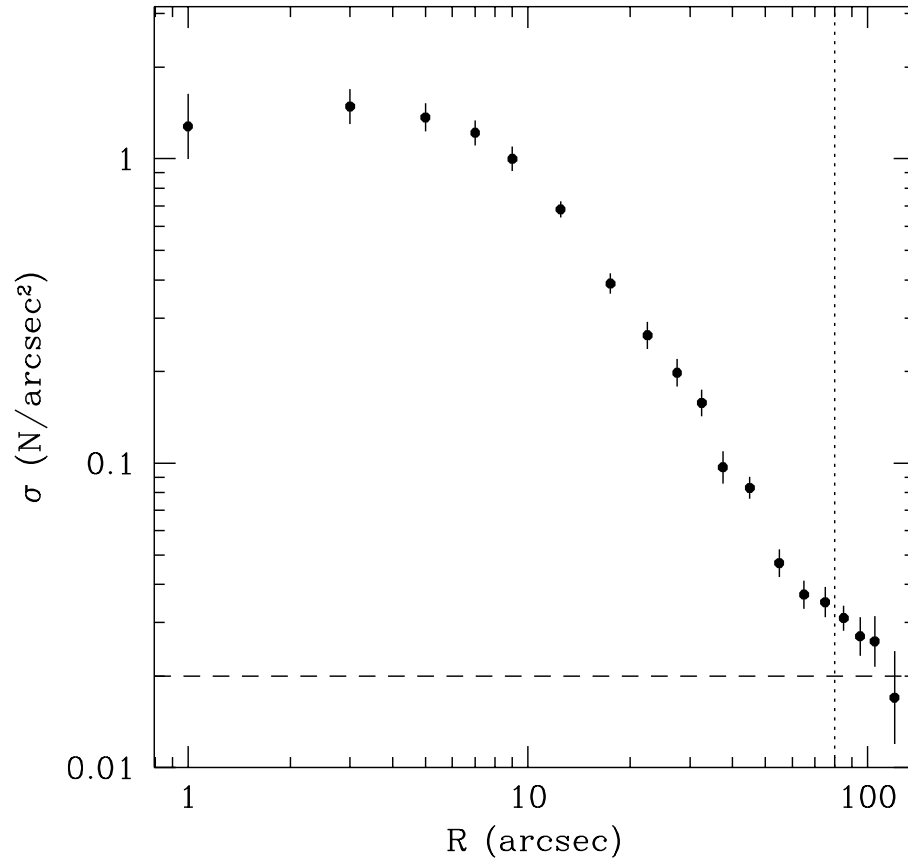


Fig. 12.— Radial surface density profile for all detected objects with $V \leq 27.0$. For $R \gtrsim 80''$ (vertical dashed line), the number density σ begins flattening off to its asymptotic background level, which we adopt as $\sigma_b = 0.02 \text{ arcsec}^{-2}$ (horizontal dashed line).

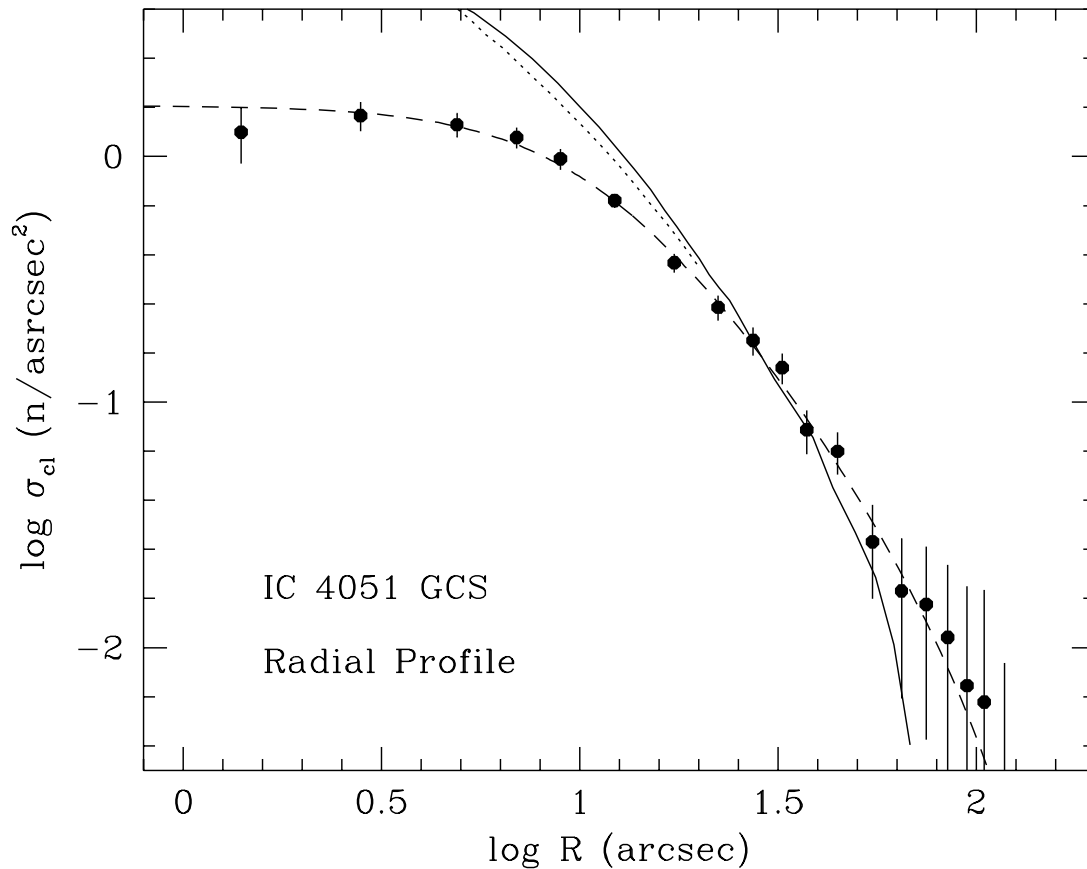


Fig. 13.— The radial projected density profile of the globular cluster system. *Solid dots* with error bars are taken from Table 7 and assume a background density $\sigma_b = 0.02 \text{ arcsec}^{-2}$. The solid line is the R -band photographic surface intensity profile of the halo light, from Strom & Strom (1978), while the dotted line is the R -band CCD profile from Jorgensen et al. (1992). Both are shifted vertically arbitrarily to match to the GCS profile. The dashed line is the best-fit King model discussed in the text, with core radius $R \simeq 10''$ and $c = 1.45$.